Protein Science (2000), *9*:1063–1072. Cambridge University Press. Printed in the USA.

Three-dimensional structures of *Drosophila melanogaster* acetylcholinesterase and of its complexes with two potent inhibitors

MICHAL HAREL,[1] GITAY KRYGER,[1] TERRONE L. ROSENBERRY,[2] WILLIAM D. MALLENDER,[2] TERENCE LEWIS,[3] RODNEY J. FLETCHER,[3] J. MITCHELL GUSS,[1,5] ISRAEL SILMAN,[4] AND JOEL L. SUSSMAN[1]

[1]Department of Structural Biology, Weizmann Institute of Science, Rehovot 76100, Israel
[2]Department of Pharmacology, Mayo Foundation for Medical Education and Research, Department of Research, Mayo Clinic Jacksonville, Jacksonville, Florida 32224
[3]Zeneca Agrochemicals, Jealott's Hill Research Station, Bracknell, Berkshire RG12 6EY, United Kingdom
[4]Department of Neurobiology, Weizmann Institute of Science, Rehovot 76100, Israel

(RECEIVED January 3, 2000; FINAL REVISION March 24, 2000; ACCEPTED March 30, 2000)

Abstract

We have crystallized *Drosophila melanogaster* acetylcholinesterase and solved the structure of the native enzyme and of its complexes with two potent reversible inhibitors, 1,2,3,4-tetrahydro-*N*-(phenylmethyl)-9-acridinamine and 1,2,3,4-tetrahydro-*N*-(3-iodophenyl-methyl)-9-acridinamine—all three at 2.7 Å resolution. The refined structure of *D. melanogaster* acetylcholinesterase is similar to that of vertebrate acetylcholinesterases, for example, human, mouse, and fish, in its overall fold, charge distribution, and deep active-site gorge, but some of the surface loops deviate by up to 8 Å from their position in the vertebrate structures, and the C-terminal helix is shifted substantially. The active-site gorge of the insect enzyme is significantly narrower than that of *Torpedo californica* AChE, and its trajectory is shifted several angstroms. The volume of the lower part of the gorge of the insect enzyme is ~50% of that of the vertebrate enzyme. Upon binding of either of the two inhibitors, nine aromatic side chains within the active-site gorge change their conformation so as to interact with the inhibitors. Some differences in activity and specificity between the insect and vertebrate enzymes can be explained by comparison of their three-dimensional structures.

Keywords: anticholinesterase; insect acetylcholinesterase; insecticide; insecticide resistance

Acetylcholinesterase (AChE) terminates synaptic transmission at cholinergic synapses by rapid hydrolysis of the neurotransmitter, acetylcholine (Rosenberry, 1975). Due to this crucial role, it serves as the target for a broad range of chemical agents, both natural and man-made (Millard & Broomfield, 1995). These anticholinesterases include drugs for the treatment of myasthenia gravis and acute glaucoma (Taylor, 1996) and, more recently, the first generation of anti-Alzheimer drugs (Davis & Powchik, 1995; Nightingale, 1997); organophosphate (OP) nerve agents (Millard & Broomfield, 1995); and OP and carbamate pesticides, including insecticides (Casida & Quistad, 1998) and anthelmintics (Martin, 1997). Crop losses worldwide due to insects have been estimated to amount to up to 50% of total agricultural output (Shani, 1998), focusing attention on the importance of insecticide development. The rapid appearance of insecticide-resistant strains (Mukhopadhyay et al., 1997) renders insecticide development a constant battle between man and insect. In the case of insecticides directed against AChE, resistance has been shown to be due to mutations in the AChE gene (Yao et al., 1997), resulting in reduced sensitivity to OP and carbamate insecticides. Knowledge of the three-dimensional (3D) structure of insect AChE can yield information crucial both to producing improved versions of existing insecticides and in the search for new candidates. Crop spraying with insecticides exposes agricultural workers to high levels of pesticides, and the WHO estimates that this leads to 220,000 deaths annually from single short-term exposure (Veil, 1992). Chronic insecticide exposure may also have substantial deleterious effects, including psychiatric symptoms and delayed neuropathy (Moretto & Lotti, 1998). Thus, insecticide design must strive for inhibitors of insect AChE that are both efficient and selective for the insect enzyme relative to human AChE (hAChE), as well as to AChEs of other vertebrates. In the following, we

Reprint requests to: Joel L. Sussman, Department of Structural Biology, Weizmann Institute of Science, Rehovot 76100, Israel; e-mail: Joel.Sussman@weizmann.ac.il.
[5]Permanent address: Department of Biochemistry, University of Sydney, Sydney 2006, Australia.

Abbreviations: AChE, acetylcholinesterase; *Dm*AChE, *Drosophila melanogaster* acetylcholinesterase; hAChE, human acetylcholinesterase; PDB, Protein Data Bank; *Tc*AChE, *Torpedo californica* acetylcholinesterase.

report the first 3D structure of an insect AChE, that of the fruit fly, *Drosophila melanogaster* (*Dm*AChE), as well as of its complexes with two members of a novel family of potent inhibitors related to the anti-Alzheimer drug, tacrine. These structures will provide a valuable tool both for insecticide design and for understanding the structural basis for mutagenic resistance to OP and carbamate insecticides. Furthermore, taken in conjunction with our knowledge of the structures of the complexes of *Torpedo californica* AChE (*Tc*AChE) with a variety of AChE inhibitors (Harel et al., 1993, 1996), and the recently reported 3D structures of mouse AChE (mAChE) (Bourne et al., 1995, 1999) and hAChE (Kryger et al., 1998), the *Dm*AChE structure will provide a rational basis for improving the selectivity of new insecticides and, thereby, reducing their toxicity toward humans and other vertebrates.

Results and discussion

Comparison of the DmAChE and TcAChE structures

Three-dimensional structures of the vertebrate AChEs, *Tc*AChE (Sussman et al., 1991), mAChE (Bourne et al., 1995, 1999), and hAChE (Kryger et al., 1998) were determined previously, and the *Dm*AChE structure reported here is the first invertebrate AChE structure to be solved. Despite the lower 36% sequence identity of *Dm*AChE and *Tc*AChE, relative to the 53–54% sequence identity of hAChE or mAChE and *Tc*AChE (Fig. 1), their 3D structures are folded similarly, and their active sites closely overlap. The main structural differences between *Dm*AChE and *Tc*AChE are found in their external loops and in the tilt of the C-terminal helix (Fig. 2A), differences that are unlikely to affect catalytic function directly.

Like the vertebrate AChEs, *Dm*AChE belongs to the α/β hydrolase fold family, with a core of eight β-sheets connected by α-helices (Ollis et al., 1992). The root-mean-square (RMS) difference in the positions of the Cα atoms of the two structures (using 362 out of 575 residues) is 0.8 Å (see Table 1). Some regions in surface loops show up to 8 Å deviation between the *Dm*AChE and *Tc*AChE structures, mostly in areas of insertions or deletions in the sequences, i.e., 22–24, 193–198, 298–301, 353–356, 418–422, and 545–549. The active-site triad (Ser238, His440, Glu367), the oxyanion hole-forming residues (Gly150, Gly151, and Ala239), and the anionic binding site (Trp 83) overlap well with the vertebrate active site. However, the side chains show slightly different conformations than those in *Tc*AChE (Fig. 2B) (for comparison to *Tc*AChE numbering, see Table 2). A change in the shape of the acyl binding pocket results from differences in two important amino acid residues: Leu328 (Phe288 in *Tc*AChE) and Phe440 (Val400 in *Tc*AChE). These changes alter the shape of the acyl pocket, but not the total space available for inhibitors or for the acyl group of the substrate (Fig. 2C).

Table 1. *Cα RMS in Å*

	*Dm*AChE	ZAI complex	ZA complex
*Dm*AChE			
ZAI complex	0.5		
ZA complex	0.7	0.4	
*Tc*AChE[a]	0.8	0.7	0.8

[a]342 Cα used.

In *Dm*AChE, as in *Tc*AChE, the dimer is formed by two symmetry-related monomers associated through a four-helix bundle. Overlapping two helices of the bundle in *Dm*AChE and *Tc*AChE in one subunit shows a slight twist of the dimers relative to each other, with the Cα atoms of *Dm*AChE Gly55 and *Tc*AChE Gly56 being the farthest apart (8.4 Å).

A comparison of insect and vertebrate AChE sequences shows three inserts in the insect sequence (Fig. 1). The two short inserts (residues 192–199 and 297–301) are located in neighboring surface loops, while the long insert (residues 104–139) is located at the surface, adjacent to the N-terminus; only four of its residues, 136–139, are visible in the electron density map, the rest being disordered.

The active-site gorge, which spans from the outer peripheral binding site, near Trp321 (Trp279 in *Tc*AChE), ~20 Å toward the catalytic triad, deep within the molecule, is wider in *Tc*AChE than in *Dm*AChE. Furthermore, the trajectory of the gorge is shifted by several angstroms (Fig. 3). This shift is the result of changes in several amino acid residues. Thus, replacement of Asp72 in *Tc*AChE by Tyr71 in *Dm*AChE, of Tyr121 in *Tc*AChE by Met153 in *Dm*AChE, and of Phe330 in *Tc*AChE by Tyr370 in *Dm*AChE, have a synergistic effect, resulting in the narrow "neck" of the gorge being shifted by up to 4.5 Å (see Figs. 3, 4). The volume of the active-site gorge below this "neck" in *Dm*AChE is about 50% of that of the equivalent portion of the gorge in *Tc*AChE, as assessed by the program VOIDOO (Kleywegt & Jones, 1994). This is due in part to a shift in the position of the indole ring of the principal "anionic" site residue, Trp83 (Figs. 2B, 3) and the replacement of Asp72 in *Tc*AChE by Tyr71 in *Dm*AChE.

The potential surface of *Dm*AChE is similar to that of other AChE molecules (Felder et al., 1997; Botti et al., 1998) and shows grouping of negative charges on the face of the molecule containing the opening to the active-site gorge and of positive charges on the opposite face (Fig. 5A). The direction of the molecular dipole moment is approximately along the axis of the active-site gorge, as is the case in other AChE structures (Fig. 5B).

Binding of inhibitors to insect AChE

The synthetic compound, 1,2,3,4-tetrahydro-*N*-(3-iodophenylmethyl)-9-acridinamine (ZAI, see Fig. 6) is a powerful anticholinesterase, with an apparent K_i = 1.09 nM for the highly homologous *Musca domestica* (house fly) AChE (C. Personeni & T. Lewis, unpubl. obs.). It makes intimate contacts with several aromatic residues in the active-site gorge of *Dm*AChE (Fig. 7A). The tacrine moiety of ZAI occupies a position in the gorge similar to that which it occupies in the *Tc*AChE:tacrine complex (Harel et al., 1993), and makes planar π–π interactions with Trp83 and Tyr370. The interplanar distances are shorter than 3.7 Å. An edge-on 3.4 Å aromatic interaction is formed between Trp472 and the saturated ring of the tacrine moiety, and there is a 3.2 Å interaction between the iodine atom and Phe330. Another π–π planar interaction, with a distance of 3.8 Å, occurs between the phenyl moiety of the inhibitor and Tyr71. An edge-on aromatic interaction of 3.9 Å occurs between the phenyl moiety and Tyr374.

Nine aromatic residues in the active-site gorge change their conformation upon insertion of the inhibitor. The side chains of residues Tyr71, Trp83, Tyr324, Phe330, Tyr370, Phe371, Tyr374, Trp472, and His480 all move so as to permit the inhibitor to be accommodated (Fig. 7B).

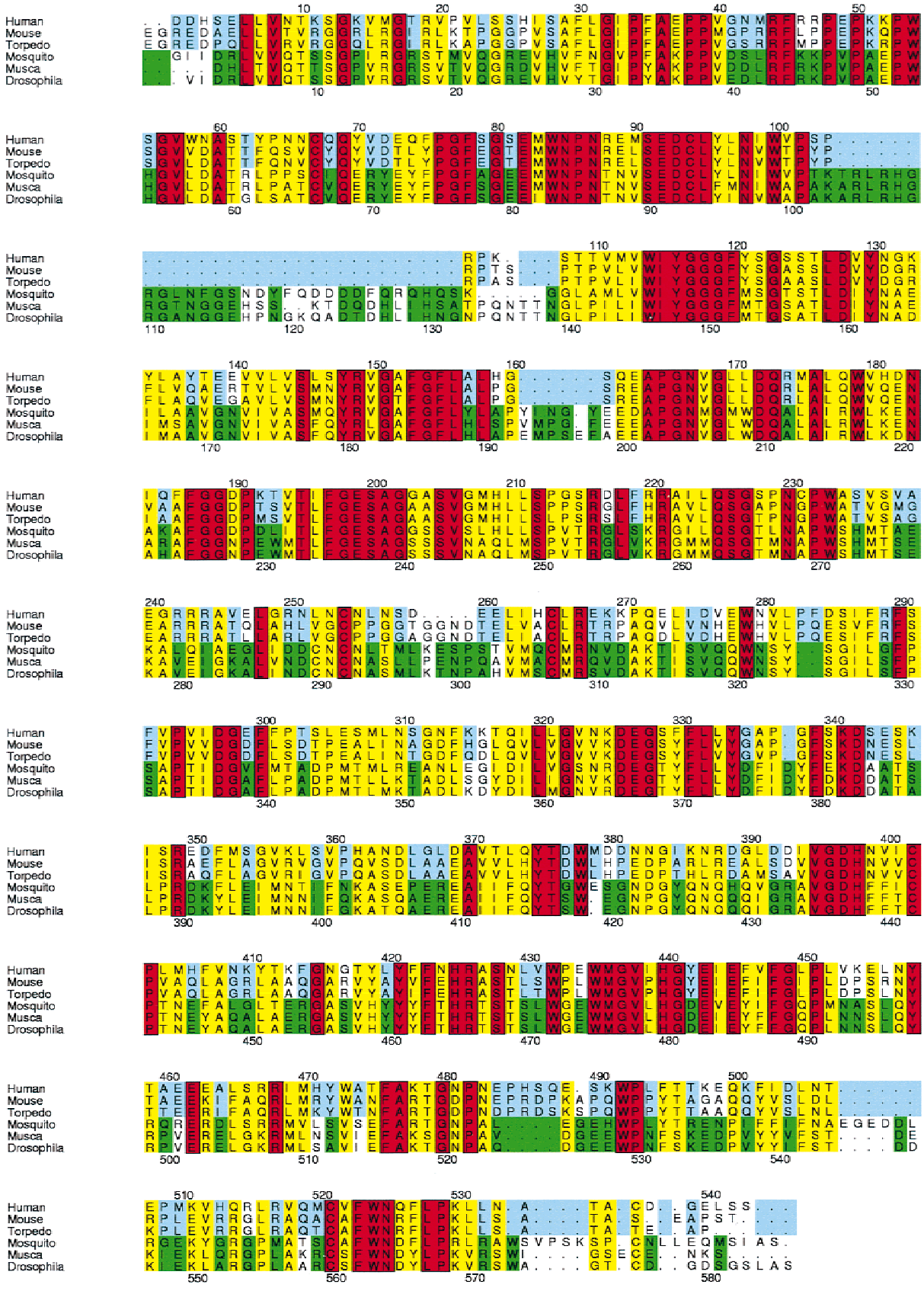

Fig. 1. Alignment of three vertebrate and three insect AChE sequences. Red, insect/vertebrate identity; yellow, insect/vertebrate similarity; blue, vertebrate only identity or similarity; green, insect only identity or similarity; *Tc*AChE numbering shown along the top line, and *Dm*AChE numbering along the bottom.

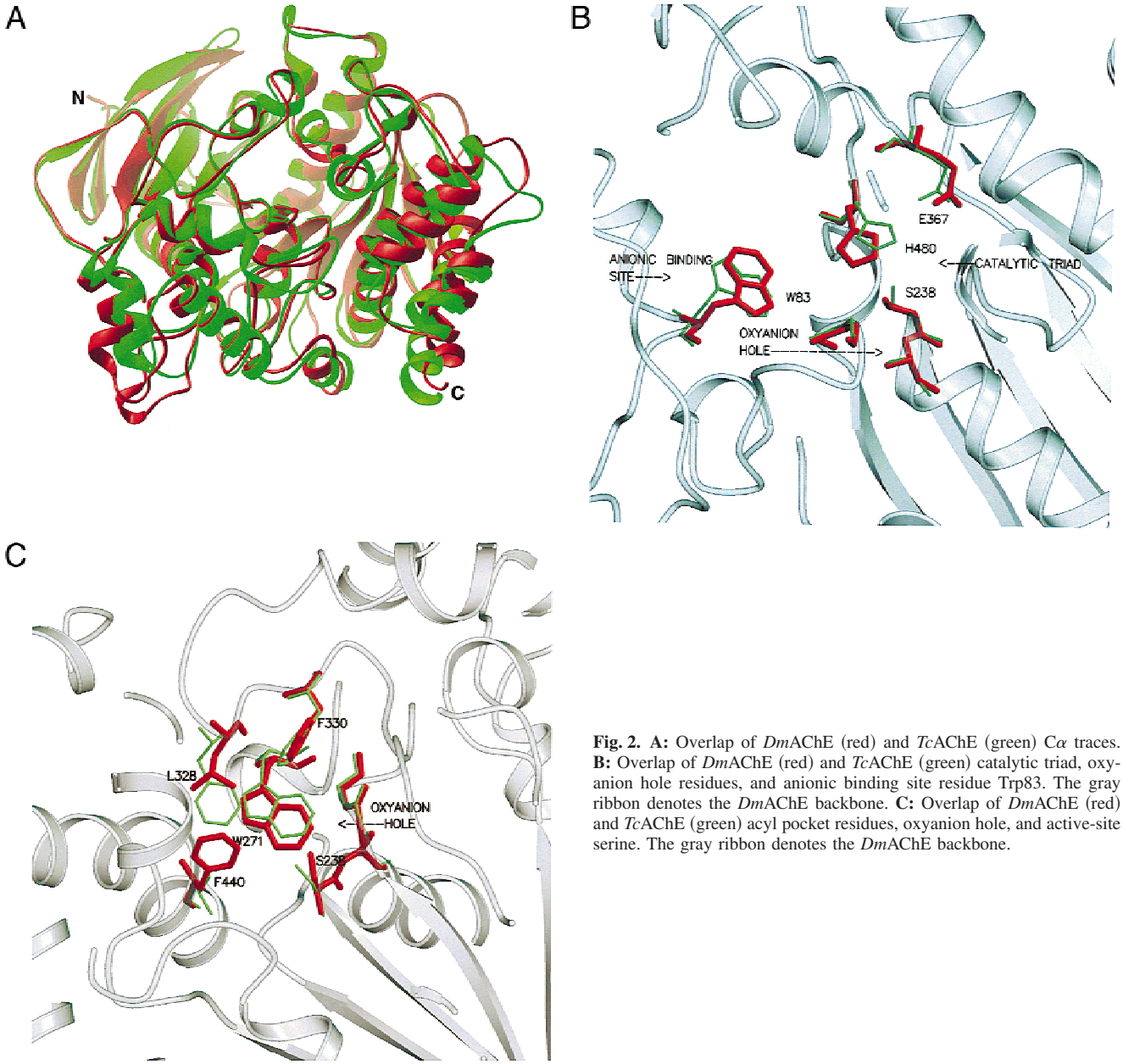

Fig. 2. A: Overlap of *Dm*AChE (red) and *Tc*AChE (green) Cα traces. **B:** Overlap of *Dm*AChE (red) and *Tc*AChE (green) catalytic triad, oxyanion hole residues, and anionic binding site residue Trp83. The gray ribbon denotes the *Dm*AChE backbone. **C:** Overlap of *Dm*AChE (red) and *Tc*AChE (green) acyl pocket residues, oxyanion hole, and active-site serine. The gray ribbon denotes the *Dm*AChE backbone.

Two peaks greater than 3.6σ are seen in the difference electron density map. The first is at the position of the iodine atom on the phenyl ring of ZAI, and the other is 1.8 Å from the catalytic triad residue, Ser238 OG. Upon refinement, the inhibitor iodine displayed a negative difference electron density peak, and a temperature factor much higher than that of the rest of the atoms in the inhibitor. Decreasing the occupancy of the iodine atom to 0.5 eliminated the negative peak and brought the temperature factor close to those of the phenyl ring atoms. This may be interpreted as implying that some of the iodine atoms are being lost. This putative cleavage, resulting in loss of ~50% of the iodine atoms, might be due to the intense X-ray radiation (Beamline XRD, Elettra Synchrotron, Trieste), causing cleavage of the C-I bond in a way analogous to cleavage of the Cys254–Cys265 bond in *Tc*AChE observed on the undulator beamline, ID14-EH4, at the European Synchrotron Radiation Facility (Grenoble) (Weik et al., 2000). We assume that the iodine is replaced by a hydroxyl group rather than by a hydrogen atom. This assumption is based on our finding that, upon refinement of the complex of *Dm*AChE with 1,2,3,4-tetrahydro-*N*-(phenylmethyl)-9-acridinamine (ZA; see Fig. 6), which lacks the iodine atom present in ZAI, the phenyl group occupies a position different from that which it occupies in the ZAI–*Dm*AChE complex, although the tacrine moiety occupies approximately the same position (see Fig. 7C). Furthermore, we do not observe disorder in the position of the iodophenyl group in ZAI–*Dm*AChE. Such disorder would be expected if the iodine were replaced by a proton, thus converting some of the ZAI molecules to ZA. A second argument in favor of I–OH exchange is the fact that in the ZAI–*Dm*AChE complex there is a water molecule 2.54 Å from the iodine atom. This distance is perfect for a –OH···water hydrogen

Table 2. *Active-site gorge residues from the bottom of the gorge to its entrance*

*Dm*AChE	*Tc*AChE
Tyr162	Tyr130
Ile484	Ile444
Tyr148	Tyr116
Glu237	Glu199
Gly481	Gly441
Gly149	Gly117
Ser238	Ser200
Gly155	Gly123
Trp83	Trp84
Gly150	Gly118
His480	His440
Thr 154	Ser122
Gly151	Gly119
Trp472	Trp432
Glu80	Ser81
Trp271	Trp233
Tyr370	Phe330
Met153[a]	Tyr121
Phe371	Phe331
Leu328	Phe288
Phe330	Phe290
Arg70[a]	Val71[a]
Tyr71	Asp72
Glu69	Tyr70
Tyr374	Tyr334
Trp321	Trp279
Glu72	Glu73
Tyr324	Leu282
Tyr73	Gln 74
Asp375	Gly33

[a]Only main-chain atoms flank the gorge.

bond, but too close for an iodine···water bond. A search through the Cambridge Data Base retrieved two well-determined X-ray structures with iodobenzene···water distances of 4.4 Å (T. Steiner, pers. comm.). While Trp83 is in the same conformation in the ZA complex as in the ZAI complex, making a π–π stacking interaction with the tacrine moiety, Tyr370 assumes a different conformation (Fig. 7C). Tyr71 is, however, in the same conformation as in the ZAI complex, though the different position of the phenyl moiety of ZA precludes it from taking part in a π–π interaction. His480 assumes two alternate conformations, both different from its conformation in the native enzyme.

The high positive difference peak seen in the oxyanion hole, near Ser238 OG, when refined as a water molecule, showed excess positive density and a temperature factor of 2 Å^2 (the minimum value specified in CNS (Brünger et al., 1997, 1998)). Although absent in the native *Dm*AChE electron density map, it is present in the ZA as well as in the ZAI complex. It was refined as a noncovalently bound sulfate ion. The assignment of sulfate to this peak was based on its tetrahedral shape and on the fact that sulfate is present in the crystallization medium.

Insect vs. vertebrate AChE: Structure-based differences in activity

The active-site gorge of AChE is coated with aromatic side chains (13 in *Dm*AChE; 14 in *Tc*AChE), which interact with its various inhibitors via noncovalent interactions (Harel et al., 1993, 1996; Kryger et al., 1999). These side chains render the gorge pliable in accommodating inhibitors by swinging to assume different conformations, thus widening or narrowing the gorge to allow passage and lodgment of inhibitors, with little or no concomitant movement of main-chain atoms. This implies that the relative narrowness of the *Dm*AChE gorge (Fig. 3A,B) cannot, as such, be taken advantage of in the design of inhibitors selective for insect AChE.

The primary candidates for achieving inhibitor selectivity are the eight residues clustered near the opening of the gorge, which differ in the insect and vertebrate sequences. The largest differences, which are potential targets for inhibitor selectivity, are in Tyr71, Tyr73, Glu80, and Asp375, which are Asp, Gln, Ser, and Gly, respectively, in vertebrates. However, differences in residues that do not line the gorge, but interact with gorge residues (i.e., second shell), may play a role in influencing selectivity, as discussed below.

One of the known differences between vertebrate and insect AChEs is the latter's ability to hydrolyze substrates with larger acyl moieties, for example, butyrylcholine (Gnagey et al., 1987). A possible reason for this difference is that in the vertebrate acyl binding pocket, the residues equivalent to Leu328 and Phe371 in *Dm*AChE (Phe288 and Phe331 in *Tc*AChE) are both phenylalanines and form a rigid π–π stacking pair. The maximal difference in dihedral angles of residue Phe331 in *Tc*AChE, and in six of its refined complexes, is $\Delta\chi1 = 11°$; $\Delta\chi2 = 13°$. In *Dm*AChE, residue 328 is a leucine, and the rigid π–π stacking is lost (though the total aromatic nature of the pocket is maintained by the "gain" of Phe440). The loss of rigid stacking renders Phe371 more mobile, thus enabling the insect acyl binding pocket to accommodate larger moieties. The corresponding maximum differences in dihedral angles for residue Phe371 in *Dm*AChE, and for four of its refined complexes (these include two recently refined unpublished complexes), are $\Delta\chi1 = 26°$; $\Delta\chi2 = 34°$. Furthermore, mutagenesis of the same residue in hAChE, i.e., Phe295Leu, increased its activity on butyrylcholine, relative to its activity on acetylcholine, by more than 100-fold (Ordentlich et al., 1993; Vellom et al., 1993). Hence, we predict that a Leu328Phe mutation in *Dm*AChE should reduce its capacity to hydrolyze butyrylcholine. This prediction will be tested by site-directed mutagenesis.

Resistance to anticholinesterase insecticides from a structural viewpoint

Four natural mutations have been identified in insect AChEs (Fournier et al., 1993; Yao et al., 1997), which confer resistance to insecticides in both *Drosophila* and in *Musca*: Gly265Ala, Phe330Tyr, Ile161Val, and Phe77Ser. (1) Gly265 is conserved across both insects and vertebrates (see Fig. 1). The Gly265Ala mutation is not in the active-site gorge, but in a second shell. We propose that the additional methyl group points toward the active-site Ser238 and thus affects catalysis. (2) The Phe330Tyr mutation is in the array of aromatics lining the acyl pocket. Phe330 is also conserved throughout other invertebrates as well as vertebrates. The additional OH of Tyr330 would be lodged in the acyl binding pocket, reduce its size, and hence its capacity to bind inhibitors. (3) The

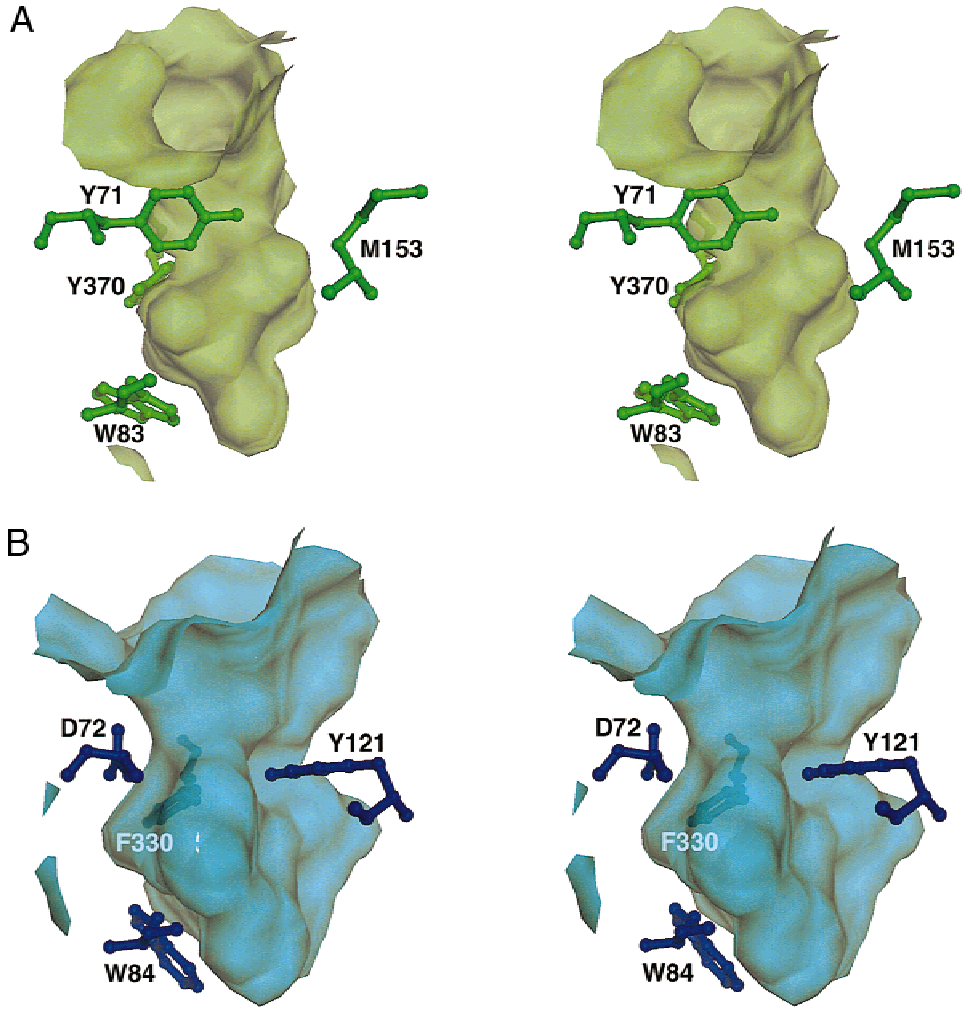

Fig. 3. Stereoviews of the active-site gorges of *Dm*AChE and *Tc*AChE. The accessible surfaces are rendered semi-transparent using the program DINO (Philippsen, 2000). Residues that significantly influence the trajectory and volume (see text) are shown as ball and stick. **A:** The active-site gorge of *Dm*AChE. **B:** The active-site gorge of *Tc*AChE. Residue Phe330 is on the far side of the surface.

Ile161Val mutation is also in the second shell. Valine is found in this position in vertebrates (see Fig. 1). Residue 161 has some interactions with the key "anionic" site residue, Trp83. Comparison of the *Dm*AChE structure with the vertebrate structures shows that the isoleucine is in somewhat closer contact than the valine with Trp83 (3.8 vs. 4.0 Å). This may have an effect on the mobility of Trp83 or on its electrostatic properties. (4) Phe77, which is another residue conserved across species, is also in the second shell. It forms an end-on π–π interaction with the active-site gorge residue Trp472; mutating it to serine eliminates this interaction and, apparently, alters the structure of the active-site gorge.

Materials and methods

Preparation of recombinant DmAChE

Construction of a secreted form of *Dm*AChE, transfection of *Drosophila* Schneider Line 2 cells, and selection of stable cell lines were accomplished as described previously (Incardona & Rosenberry, 1996). The S2-SEC 1/3 clone was maintained at high cell density in Schneider's *Drosophila* medium (Life Technologies, Inc., Rockville, Missouri) for production of secreted *Dm*AChE. Medium was removed every 10–14 days, and *Dm*AChE was purified by two cycles of affinity purification on an acridinium resin (Rosenberry & Scoggin, 1984). Briefly, after loading the *Dm*AChE-medium over a 15–50 mL affinity column, the resin was washed with buffers containing 10 mM sodium phosphate, pH 7, in four stages, to remove impurities. The four buffers consisted of (1) 5–10 column volumes of 10 mM sodium phosphate, pH 7, only; (2) two to three column volumes of buffer with the addition of 500 mM NaCl; (3) 5–10 column volumes of buffer with 50 mM NaCl and 0.1% Triton X-100 added; (4) 5–10 column volumes of buffer with the addition of 20 mM NaCl. Purified *Dm*AChE was eluted from the column by ligand competition, using a solution of 5 mM sodium phosphate, pH 7, containing 5 mM decamethonium bromide (Sigma Chemical Co., St. Louis, Missouri), and 0.1% Triton X-100. Fractions containing purified *Dm*AChE were identified by a spectrophotometric activity assay (Ellman et al., 1961) and pooled for dialysis against 10 mM sodium phosphate, pH 7, to remove the decamethonium. The enzyme was then subjected to a

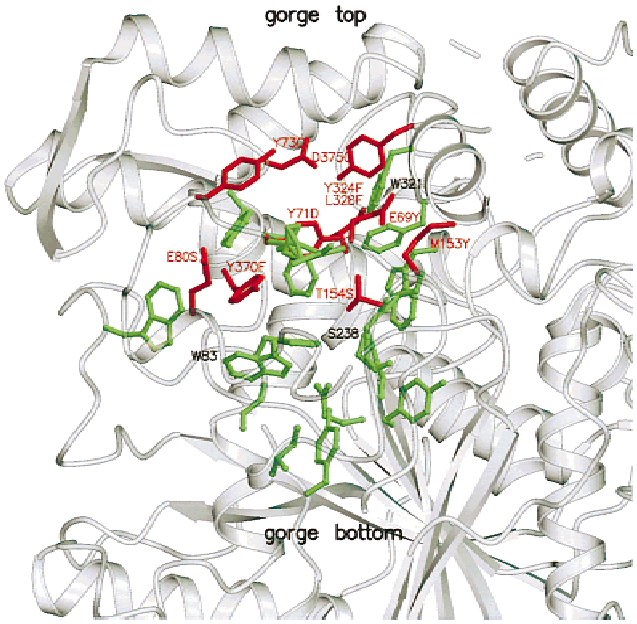

Fig. 4. Active-site gorge flanking residues in *Dm*AChE. Residues identical in vertebrate and insect are shown in green; different residues shown in red. For those residues labeled, the letter preceding the residue number corresponds to *Dm*AChE, and the letter following it corresponds to *Tc*AChE.

second round of affinity purification, using the same washing protocol, but eluting with a decamethonium solution that did not contain Triton X-100. Purified recombinant *Dm*AChE samples analyzed by SDS-polyacrylamide gel electrophoresis (Laemmli, 1970) displayed no detectable contaminants. In the presence of reducing agents, a prominent band of 70 kDa monomer and minor bands corresponding to 55 and 16 kDa fragments were obtained. The smaller fragments are the result of the same proteolytic processing observed for native *Dm*AChE (Gnagey et al., 1987). In the absence of reducing agents, bands of 140 kDa homodimers (viz. two 70 kDa subunits) and 125 kDa heterodimers (viz. one 70 kDa subunit and one 55 kDa fragment) were seen (Incardona & Rosenberry, 1996).

Data collection, structure determination, and refinement

*Dm*AChE crystals were grown by the hanging drop method at 19 °C from a 4 mg/mL protein solution diluted 1:1 with the reservoir solution, whose composition was 13% MPEG2000/0.1 M ammonium sulfate/0.03 M leucine/0.1 M acetate, pH 4.6. Crystals grew in four to five days as trigonal prisms, 0.2 mm in size, space group $P4_32_12$ (enantiomorph chosen from the structure solution). The crystals of the complexes were obtained by cocrystallization. In the case of ZAI (Fig. 6), the mother liquor contained 2% of a saturated solution of the ligand in DMSO; in the case of ZA, it contained 2% of a saturated solution of the ligand in 75% methanol. In both cases, the crystals obtained were isomorphous with the native *Dm*AChE crystals (see Table 3).

X-ray data for the native crystal and for the ZAI complex were collected at the Elettra synchrotron in Trieste, on beamline XRD, at 100 K, using 20% sucrose as cryoprotectant. The data were

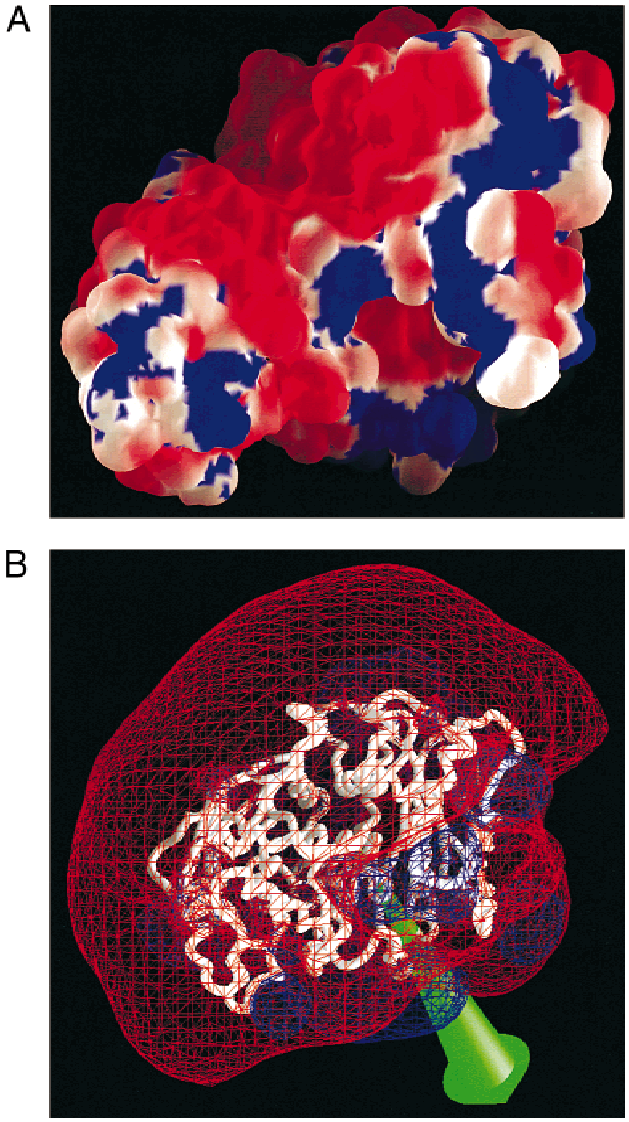

Fig. 5. A: Representation of solvent-accessible molecular surface. The entrance to the active-site gorge is centered within the large red area near the top left. Color coding represents electrostatic potential surfaces: 2.5 kT/e in blue and −2.5 kT/e in red. **B:** Schematic drawing of the ±0.25 kT/e isopotential surface of *Dm*AChE. Orientation is the same as in **A**, and the green arrow denotes the direction of the dipole moment.

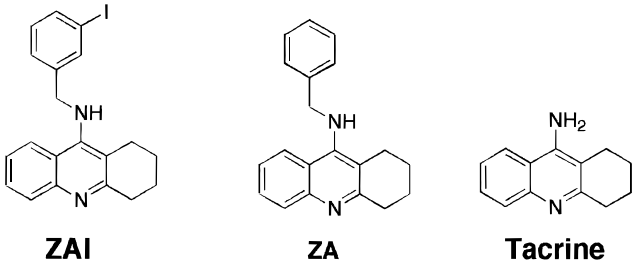

Fig. 6. Chemical formulas of reversible AChE inhibitors: ZAI, ZA, and tacrine.

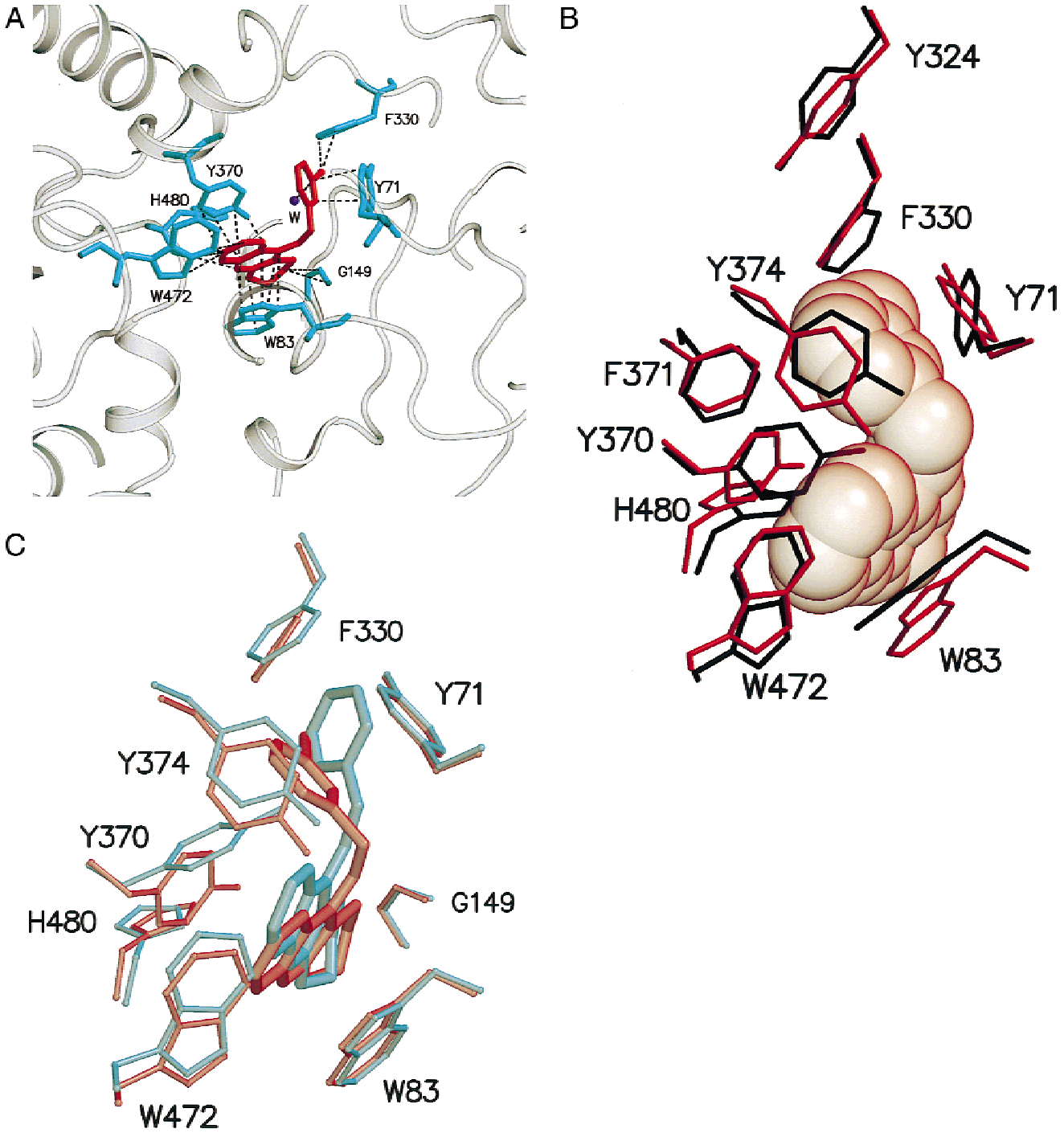

Fig. 7. Representations of interactions of *Dm*AChE with ZAI and ZA. **A:** *Dm*AChE residues (turquoise) interacting with ZAI (red) with distances <3.8 Å. **B:** Nine aromatic residues in native *Dm*AChE (black) change their conformation when ZAI (red), shown with its van der Waals surface, binds to *Dm*AChE. **C:** Overlap of ZAI complex (red) and ZA complex (turquoise). The inhibitors are shown as thick sticks, and the side chains of the principal residues with which they interact as thin sticks.

integrated, scaled, and reduced with DENZO and SCALEPACK (Otwinowski & Minor, 1997). A molecular replacement solution was found using the program AMoRe (Navaza, 1994) of the program suite CCP4 (Bailey, 1994).

The solution, using the *Tc*AChE monomer as a search model, and 10 − 4 Å resolution data, showed a monomer in the asymmetric unit, with *R*-factor = 53%, correlation coefficient = 30%. The packing in space group $P4_32_12$ reveals the familiar AChE dimer (Sussman et al., 1991), with a disulfide bridge between the COOH-terminal Cys577 residues. Despite a sequence identity of *Dm*AChE to *Tc*AChE and to hAChE of 37 and 36%, respectively (Fig. 1), refinement of the *Dm*AChE structure, starting from the

Table 3. *Data collection and refinement*

	Native	Complex ZAI	Complex ZA	Derivative Xe
Space group, mol/AU	$P4_32_12$, 1	$P4_32_12$, 1	$P4_32_12$, 1	$P4_32_12$, 1
Unit cell axes $a = b, c$ (Å)	94.34, 159.0	94.93, 160.02	95.81, 162.03	94.33, 158.9
X-ray source	Elettra, Trieste, XRD	Elettra, Trieste, XRD	NSLS, BNL, X12C	Elettra, Trieste, XRD
Wavelength (Å)	1.0	1.0	0.98	1.0
Resolution range (Å)	30–2.70	30–2.72	30–2.70	30–2.72
Data collection temperature (K)	100	100	100	100
Cryoprotectant	20% sucrose	20% sucrose	20% sucrose	20% sucrose
No. of unique reflections	20,200	19,982	21,076	20,182
Completeness (%)	99.1 (98.8)[a]	96.8 (99.2)[a]	97.7 (84.4)[a]	99.3 (99.9)[a]
R_{sym} (on I) (%)	5.0 (16.1)[a]	6.0 (25.4)[a]	3.8 (27.4)[a]	6.3 (39.5)[a]
$I/\sum(I)$	33.5 (5.8)[a]	15.5 (2.4)[a]	24.3 (3.2)[a]	23.7 (3.7)[a]
Rcullis (centric)	—	—	—	73%
Phasing power (centric)	—	—	—	0.87
Rcullis (acentric)	—	—	—	83%
Phasing power (acentric)	—	—	—	1.20
Figure of merit (centric)	—	—	—	0.52
No. of protein atoms	4,216	4,246	4,207	—
No. of solvent atoms	137	165	97	—
No. of sugars	6	5	5	—
No. of sulfate ions	—	1	1	—
R_{fact} (R_{free}) $F > 0\sigma$	25.8% (30.1%)	22.0% (26.5%)	22.0% (26.3%)	—
RMS from ideality[b]				
Bond length (Å)	0.009	0.008	0.007	—
Bond angle (Å)	1.670	1.425	1.463	—
Average B values (Å^2)	53.8	53.3	50.8	—
Ramachandran plot[c]				
Favord	77.2%	84.9%	85.1%	—
Allowed	20.9%	13.7%	13.7%	—
Generously allowed	1.7%	0.9%	0.9%	—
Disallowed	0.2%	0.7%	0.4%	—

[a]Statistics for outer shell 2.8–2.7 Å data in parentheses.
[b]Calculated by program WHATCHECK (Vriend, 1990).
[c]Calculated by program PROCHECK (Laskowski et al., 1993).

*Tc*AChE model (Raves et al., 1997) (PDB IDCode 2ACE), resulted in a model whose *R*-factor did not refine below 35%.

A single suitable heavy atom derivative was found by immersing a native *Dm*AChE crystal in a chamber containing gaseous xenon at 5 bar pressure for 1 min, as described by Sauer and coworkers (Sauer et al., 1997). X-ray data were collected as described above for the native crystal. The crystal of the Xe derivative was isomorphous with the native crystal (see Table 3). The locations of two Xe atoms were determined with the program FFT and refined with the program MLPHARE, from the program suite CCP4 (Bailey, 1994), and with HEAVY_SEARCH from the program suite CNS (Brünger et al., 1997, 1998). Both programs yielded the same two Xe sites, which were used for the phasing with their anomalous contribution (Table 3). The ZAI complex, which contains iodine, was designed and synthesized to aid in phasing; it did not, however, yield useful heavy atom phasing information and was solved and refined in parallel to the native structure.

The structures were refined in the resolution range of 30–2.7 Å, using the maximum likelihood, slow cooling, and optimum combination of coordinate files that produced a minimum free *R*-value from the averaged structure factors using the CNS package (Brünger et al., 1997, 1998). The Fobs were scaled anisotropically, and a bulk solvent correction was applied (Brünger et al., 1997, 1998). Of particular help in solution of the structure was the composite anneal omit map produced by CNS (Brünger et al., 1997, 1998).

The structures were fitted into the electron density with the program O (Jones et al., 1991). Residues 1–2, 104–135, 575–586 in the native *Dm*AChE structure, residues 103–135, 574–586 in the ZAI complex structure, and residues 1–2, 103–136, 574–586 in the ZA complex do not lie in any significant electron density. The largest insert in the *Dm*AChE sequence, relative to *Tc*AChE, is residues 104–140 (Fig. 1). No electron density is observed for this insert, except for four residues at its C-terminus.

Because the refined *Dm*AChE-ZAI complex structure showed some unexplained electron density at the active site, a similar inhibitor, ZA, in which the iodine atom had been replaced by a hydrogen (Fig. 6), was cocrystallized with *Dm*AChE. X-ray data were collected on beamline X12C of the NSLS, at Brookhaven National Laboratory, at a wavelength of 0.98 Å, at 100 K, using 20% sucrose as cryoprotectant. This structure was solved by molecular replacement, starting from the *Dm*AChE-ZAI structure.

The refined structures were analyzed with program PROCHECK (Laskowski et al., 1993). The figures were generated with the programs ALSCRIPT (Barton, 1993), MOLSCRIPT (Kraulis, 1991), BOBSCRIPT (Esnouf, 1999), DINO (Philippsen, 2000), GRASP (Nicholls et al., 1991), and RASTER3D (Merritt & Bacon, 1997).

The atomic coordinates and structure factors for the native structure, and for the complexes with ZAI and ZA have been deposited at the PDB and have ID codes 1qo9, 1qon, and 1dx4, respectively.

Acknowledgments

This work was supported by the U.S. Army Medical Research Acquisition Activity under Contract No. DAMD17-97-2-7022, the European Union IVth Framework in Biotechnology, the Kimmelman Center for Biomolecular Structure and Assembly, Israel, the Nella and Leon Benoziyo Center for Neurosciences, the Dana Foundation, and the generous support of Tania Friedman. T.L.R. and W.D.M. acknowledge the support of NIH Grant NS-16577. I.S. is Bernstein–Mason Professor of Neurochemistry. Special thanks to Cristoph Kratky, Oliver Sauer, and Ulrike Wagner (University of Graz), for helping us to obtain the Xe heavy atom derivative, and Ansgar Philippsen for help in preparation of the figures.

References

Bailey S. 1994. The CCP4 suite: Programs for protein crystallography. *Acta Crystallogr D50*:760–763.

Barton GJ. 1993. ALSCRIPT, a tool to format multiple sequence alignments. *Protein Eng 6*:37–40.

Botti SA, Felder CE, Sussman JL, Silman I. 1998. Electrotactins: A class of adhesion proteins with conserved electrostatic and structural motifs. *Protein Eng 11*:415–420.

Bourne Y, Taylor P, Bougis PE, Marchot P. 1999. Crystal structure of mouse acetylcholinesterase. A peripheral site-occluding loop in a tetrameric assembly. *J Biol Chem 274*:2963–2970.

Bourne Y, Taylor P, Marchot P. 1995. Acetylcholinesterase inhibition by fasciculin: Crystal structure of the complex. *Cell 83*:503–512.

Brünger AT, Adams PD, Clore GM, DeLano WL, Gros P, Grosse-Kunstleve RW, Jiang JS, Kuszewski J, Nilges M, Pannu NS, et al. 1998. Crystallography & NMR system: A new software suite for macromolecular structure determination. *Acta Crystallogr D54*:905–921.

Brünger AT, Adams PD, Rice LM. 1997. New applications of simulated annealing in X-ray crystallography and solution NMR. *Structure 5*:325–336.

Casida JE, Quistad GB. 1998. Golden age of insecticide research: Past, present, or future? *Annu Rev Entomol 43*:1–16.

Davis KL, Powchik P. 1995. Tacrine. *Lancet 345*:625–630.

Ellman GL, Courtney KD, Andres V Jr, Featherstone RM. 1961. A new and rapid colorimetric determination of acetylcholinesterase activity. *Biochem Pharmacol 7*:88–95.

Esnouf RM. 1999. Further additions to MolScript version 1.4, including reading and contouring of electron-density maps. *Acta Crystallogr D55*:938–940.

Felder CE, Botti SA, Lifson S, Silman I, Sussman JL. 1997. External and internal electrostatic potentials of cholinesterase models. *J Mol Graphics Modelling 15*:318–327.

Fournier D, Mutero A, Pralavorio M, Bride J-M. 1993. *Drosophila* acetylcholinesterase: Mechanisms of resistance to organophosphates. *Chem Biol Interact 87*:233–238.

Gnagey AL, Forte M, Rosenberry TL. 1987. Isolation and characterization of acetylcholinesterase from *Drosophila*. *J Biol Chem 262*:13290–13298.

Harel M, Quinn DM, Nair HK, Silman I, Sussman JL. 1996. The X-ray structure of a transition state analog complex reveals the molecular origins of the catalytic power and substrate specificity of acetylcholinesterase. *J Am Chem Soc 118*:2340–2346.

Harel M, Schalk I, Ehret-Sabatier L, Bouet F, Goeldner M, Hirth C, Axelsen P, Silman I, Sussman JL. 1993. Quaternary ligand binding to aromatic residues in the active-site gorge of acetylcholinesterase. *Proc Natl Acad Sci USA 90*:9031–9035.

Incardona JP, Rosenberry TL. 1996. Construction and characterization of secreted and chimeric transmembrane forms of *Drosophila* acetylcholinesterase: A large truncation of the C-terminal signal peptide does not eliminate glycoinositol phospholipid anchoring. *Mol Biol Cell 7*:595–611.

Jones TA, Zou J-Y, Cowan SW, Kjeldgaard M. 1991. Improved methods for building protein models in electron density maps and the location of errors in these models. *Acta Crystallogr A47*:110–119.

Kleywegt GJ, Jones TA. 1994. Detection, delineation, measurement and display of cavities in macromolecular structures. *Acta Crystallogr D50*:178–185.

Kraulis P. 1991. MOLSCRIPT: A program to produce both detailed and schematic plots of protein structure. *J Appl Crystallogr 24*:946–950.

Kryger G, Giles K, Harel M, Toker L, Velan B, Lazar A, Kronman C, Barak D, Ariel N, Shafferman A, et al. 1998. 3D Structure at 2.7Å resolution of native and E202Q mutant human acetylcholinesterase complexed with fasciculin-II. In: Doctor BP, Taylor P, Quinn DM, Rotundo RL, Gentry MK, eds. *Structure and function of cholinesterases and related proteins*. New York: Plenum. pp 323–326.

Kryger G, Silman I, Sussman JL. 1999. Structure of acetylcholinesterase complexed with E2020 (Aricept®): Implications for the design of new anti-Alzheimer drugs. *Structure 7*:297–307.

Laemmli UK. 1970. Cleavage of structural proteins during the assembly of the head of bacteriophage T4. *Nature 227*:680–685.

Laskowski RA, MacArthur MW, Moss D, Thornton JM. 1993. PROCHECK: A program to check the stereochemical quality of protein structures. *J Appl Crystallogr 26*:283–291.

Martin RJ. 1997. Modes of action of anthelmintic drugs. *Vet J 154*:11–34.

Merritt EA, Bacon DJ. 1997. Raster3D—Photorealistic molecular graphics. *Methods Enzymol 277*:505–524.

Millard CB, Broomfield CA. 1995. Anticholinesterases: Medical applications of neurochemical principles. *J Neurochem 64*:1909–1918.

Moretto A, Lotti M. 1998. Poisoning by organophosphorus insecticides and sensory neuropathy. *J Neurol Neurosurg Psychiatry 64*:463–468.

Mukhopadhyay AK, Karmakar P, Hati AK, Dey P. 1997. Recent epidemiological status of malaria in Calcutta Municipal Corporation area, West Bengal. *Indian J Malariol 34*:188–196.

Navaza J. 1994. AMoRe—An automated procedure for molecular replacement. *Acta Crystallogr D50*:157–163.

Nicholls A, Sharp K, Honig B. 1991. Protein folding and association: Insights from the interfacial and thermodynamic properties of hydrocarbons. *Proteins Struct Funct Genet 11*:281–296.

Nightingale SL. 1997. Donepezil approved for treatment of Alzheimer's disease. *JAMA 277*:10.

Ollis DL, Cheah E, Cygler M, Dijkstra B, Frolow F, Franken SM, Harel M, Remington SJ, Silman I, Schrag J, et al. 1992. The α/β hydrolase fold. *Protein Eng 5*:197–211.

Ordentlich A, Barak D, Kronman C, Flashner Y, Leitner M, Segall Y, Ariel N, Cohen S, Velan B, Shafferman A. 1993. Dissection of the human acetylcholinesterase active center—Determinants of substrate specificity—Identification of residues constituting the anionic site, the hydrophobic site, and the acyl pocket. *J Biol Chem 268*:17083–17095.

Otwinowski Z, Minor W. 1997. Processing of X-ray diffraction data collected in oscillation mode. *Methods Enzymol 276*:307–326.

Philippsen A. 2000. DINO: Visualizing structural biology. http://www.bioz.unibas.ch/~xray/dino.

Raves ML, Harel M, Pang Y-P, Silman I, Kozikowski AP, Sussman JL. 1997. 3D Structure of acetylcholinesterase complexed with the nootropic alkaloid, (-)-huperzine A. *Nat Struct Biol 4*:57–63.

Rosenberry TL. 1975. Acetylcholinesterase. *Adv Enzymol 43*:103–218.

Rosenberry TL, Scoggin DM. 1984. Structure of human erythrocyte acetylcholinesterase. *J Biol Chem 259*:5643–5652.

Sauer O, Schmidt A, Kratky C. 1997. Freeze-trapping isomorphous xenon derivatives of protein crystals. *J Appl Crystallogr 30*:476–486.

Shani A. 1998. Integrated pest management using pheromones. *Chemtech 28*:30–35.

Sussman JL, Harel M, Frolow F, Oefner C, Goldman A, Toker L, Silman I. 1991. Atomic structure of acetylcholinesterase from *Torpedo californica*: A prototypic acetylcholine-binding protein. *Science 253*:872–879.

Taylor P. 1996. Anticholinesterase agents. In: Hardman JG, Limbird LE, Molinoff PB, Ruddon RW, Gilman AG, eds. *The pharmacological basis of therapeutics,* 9th ed. New York: McGraw-Hill. pp 161–176.

Veil S. 1992. *Our planet, our health*. New York: WHO Commission on Health and Environment, World Health Organization.

Vellom DC, Radic Z, Li Y, Pickering NA, Camp S, Taylor P. 1993. Amino acid residues controlling acetylcholinesterase and butyrylcholinesterase specificity. *Biochemistry 32*:12–17.

Vriend G. 1990. WHAT IF: A molecular modelling and drug design program. *J Mol Graphics Modelling 8*:52–56.

Weik M, Ravelli RBG, Kryger G, McSweeney S, Raves M, Harel M, Gros P, Silman I, Kroon J, Sussman JL. 2000. Specific chemical and structural damage to proteins produced by synchrotron radiation. *Proc Natl Acad Sci USA 97*:623–628.

Yao H, Chuanling Q, Williamson MS, Devonshire AL. 1997. Characterization of the acetylcholinesterase gene from insecticide-resistant houseflies (*Musca domestica*). *Chin J Biotechnol 13*:177–183.